Korean J. Chem. Eng., 40(3), 473-487 (2023)
DOI: 10.1007/s11814-022-1372-0

pISSN: 0256-1115
eISSN: 1975-7220

INVITED REVIEW PAPER

A short review of the recent developments in functional separators for lithium-sulfur batteries

Donghyeok Son‡, Won-Gwang Lim‡, and Jinwoo Lee†

Department of Chemical and Biomolecular Engineering, Korea Advanced Institute of Science and Technology (KAIST), 291 Daehak-ro, Yuseong-gu, Daejeon 34141, Korea

(*Received 31 August 2022 • Revised 31 October 2022 • Accepted 8 December 2022*)

Abstract−Recently, interest in batteries with high energy density has greatly increased as a result of the sharp rise in demand for electric vehicles, which are needed to achieve carbon neutrality by the year 2050. Lithium-sulfur (Li-S) batteries are emerging as the next-generation batteries owing to their high theoretical energy density of 2,600 W h kg^{-1}. However, they are difficult to commercialize because of various hurdles, including the high reactivity of Li metal anode, shuttle phenomenon, and slow sulfur conversion reactions at the cathode. The development of advanced functional separators fabricated by coating functional materials on the surface of separators is one of the most promising strategies to tackle these issues and push Li-S battery performance to higher levels. The control of the physical and chemical properties of coating materials allows functional separators to exhibit multiple effects favorable for addressing the intrinsic issues of Li-S batteries, which is beyond the conventional role of general separators. Therefore, this review provides a comprehensive overview of the recent developments in functional separators for high-performance Li-S batteries.

Keywords: Lithium-sulfur Batteries, Functional Separators, Shuttle Phenomenon, Electrocatalysis

INTRODUCTION

Owing to the rising demand for portable electronics and electric vehicles, interest in energy storage devices has increased [1-4]. Recently, a number of intrinsic limitations of conventional lithium-ion batteries (LIBs) have been revealed, including low theoretical energy density, high cost of cathode materials, and lack of environmental friendliness [5-9]. Therefore, developing next-generation batteries that outperform LIBs is essential. In this regard, Li-S batteries comprising Li metal anode and sulfur cathode have attracted considerable attention owing to their promising advantages. First, the high gravimetric capacity of the electrode materials enables the achievement of a high theoretical gravimetric energy density of 2,600 W h kg^{-1}. Second, sulfur (cathode material) is a naturally abundant material. Thus, the cost of sulfur (~$150 per ton) is much lower than that of cobalt (~$3,300 per ton), making it suitable as core material for the cathode of LIBs [10-12].

However, despite these advantages, Li-S batteries have a number of issues in the cathode to be commercialized: For the last 10 years, i) the low electrical conductivity of sulfur (5×10^{-30} S cm^{-1}) and Li_2S (10^{-13} S cm^{-1}) at room temperature [13,14]; ii) large volume change (180%) between sulfur and Li_2S during the discharge and charge process [15]; iii) shuttle phenomenon caused by electrolyte-soluble lithium polysulfides (*i.e.*, Li_2S_x, $4\leq x\leq 8$), which diffuse from the cathode to the anode due to the concentration gradient [16-18]; and iv) sluggish reaction kinetics for the nucleation and dissociation of Li_2S [19,20]. Various approaches to address these issues have been reported for realizing advanced Li-S batteries with high reversible capacity, Coulombic efficiency, and cycling stability. For example, the development of conductive host materials [21-23], adsorption materials [24,25], and electrocatalysts [26,27] has been intensively studied for cathodes. Consequently, the performance of Li-S batteries has been efficiently improved over the past decade. However, the shuttle phenomenon caused by the crossover of lithium polysulfides (LiPSs) within the electrolyte has not been completely addressed by the development of these advanced electrode materials for both the cathode and anode.

Recently, extensive research has been conducted on the design of functional separators to overcome the limitations of electrode material design strategies and boost the Li-S battery performance to the highest level. A separator is an electrochemically inactive but essential component of rechargeable batteries. The conventional role of the separator is to prevent direct electron transfer between the cathode and anode but allow cations to pass through the battery system selectively. Functional separators fabricated by coating functional materials on the surface of conventional separators enable the control of the physical and chemical properties of separators, leading to a variety of multi-effects desirable for high-performance Li-S batteries.

In this regard, the design of advanced functional separators beyond the conventional role of separators is one of the most promising strategies to achieve the research goal of Li-S batteries, including high gravimetric energy density and cycling stability comparable to LIBs. Therefore, a comprehensive understanding of the relationship between the physical and chemical properties of functional separators and the Li-S cell performance is required. This review presents an insightful overview of state-of-the-art advances

†To whom correspondence should be addressed.
E-mail: jwlee1@kaist.ac.kr
‡These authors contributed to this work equally.

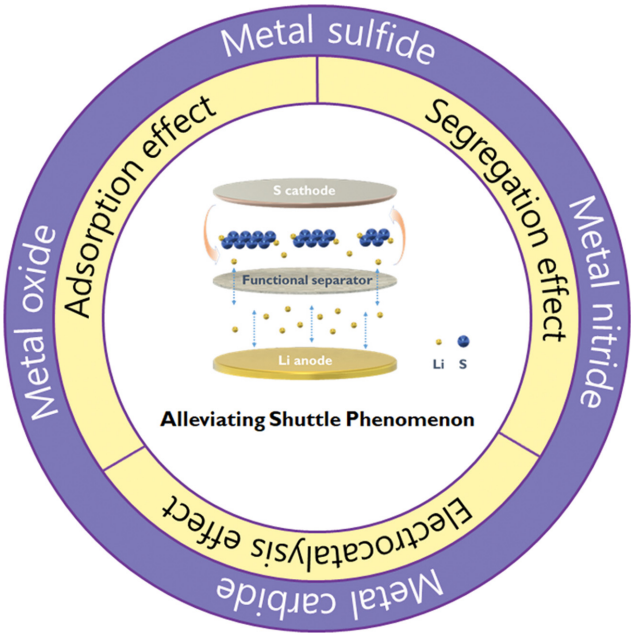

Fig. 1. Schematic diagram of suppressing shuttle phenomenon through functional separator in Li-S batteries.

in the development of functional separators in the research field of Li-S batteries, including the additional role and mechanical details of functional separators for the redox reaction of LiPSs, and our perspectives on future research directions to fabricate functional separators for Li-S batteries (Fig. 1).

WORKING PRINCIPLE AND ISSUES OF Li-S BATTERIES

During the operation of Li-S batteries, two phases are involved in the electrochemical reactions of sulfur and Li^+ ions: liquid and solid (Fig. 2(a)). In particular, a sulfur atom from elemental sulfur (S_8) can electrochemically react with two Li^+ ions in the reduction reaction, producing lithium sulfide (Li_2S) during the discharge process, as follows:

$$\text{Cathode: } S_8 + 16Li^+ + 16e^- \rightarrow 8Li_2S$$
$$\text{Anode: } 16Li^0 \rightarrow 16Li^+ + 16e^-$$

For this reduction reaction, two separate plateaus are discernible at approximately 2.3 V and 2.1 V (*vs.* Li/Li^+). At the upper plateau at 2.3 V, the reduction of S_8 to electrolyte-soluble LiPSs (*i.e.*, Li_2S_8 and Li_2S_6) occurs stepwise *via* a solid-liquid reaction (Fig. 2(b)). In the subsequent slope region, a further reduction from Li_2S_6 to Li_2S_4 occurs *via* a liquid-liquid reaction. The theoretical capacity for reducing S_8 to Li_2S_4 (Q_H) is 418 mA h g^{-1}, which is 25% of the total theoretical discharge capacity of Li-S electrochemistry [3,28]. In the lower plateau region (2.1 V), Li_2S_4 is further reduced to Li_2S_2 and Li_2S, the electrolyte-insoluble discharge products, *via* a liquid-solid reaction. The theoretical capacity for the conversion of Li_2S_4 to Li_2S (Q_L) is 1,254 mA h g^{-1}, which is 75% of the total discharge capacity [29,30].

For the charging process, the final discharge product Li_2S is electrochemically oxidized to LiPSs, followed by the formation of the final charge product S_8, as follows:

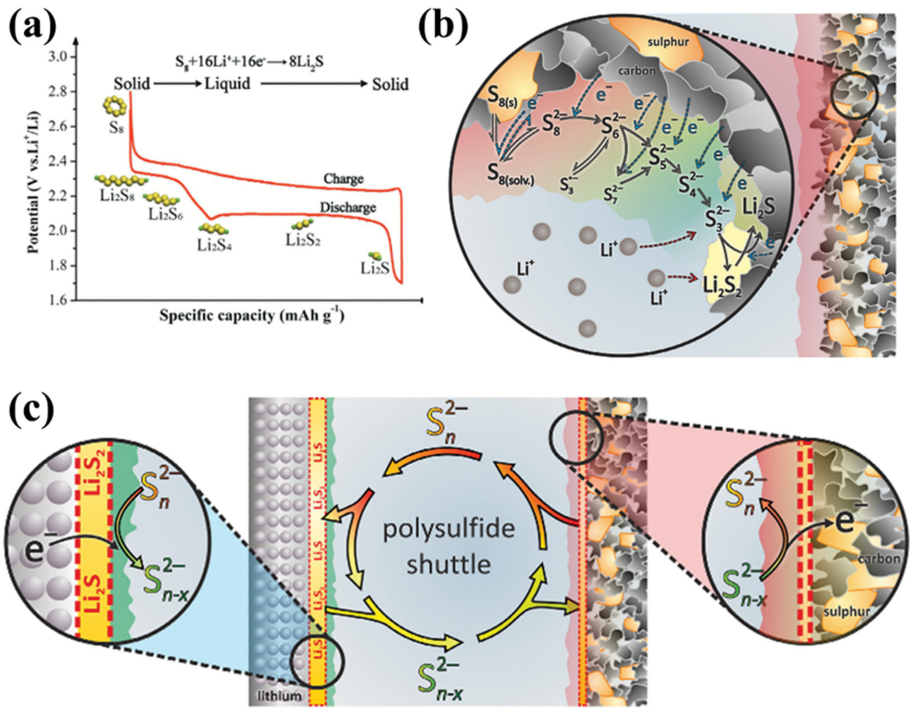

Fig. 2. (a) Typical discharge/charge voltage profile of Li-S batteries (reproduced with permission from Ref. [3]). (b) Subsequent reduction reaction of S_8 to insoluble Li_2S_2/Li_2S. (c) Graphical depiction of shuttle phenomenon by diffusion of soluble intermediate polysulfides between cathode and anode during charge/discharge operation (reproduced with permission from Ref. [32]).

Cathode: $8Li_2S \rightarrow S_8 + 16Li^+ + 16e^-$
Anode: $16Li^+ + 16e^- \rightarrow 16Li^0$

During the first sharp increase in potential at the beginning of the charging process, solid Li_2S is decomposed to form liquid LiPSs (*e.g.*, Li_2S_4). In the potential range of 2.4-2.5 V, a reversible conversion reaction from LiPSs (*e.g.*, Li_2S_6 and Li_2S_8) to S_8 occurs [31]. During the discharge/charge process, the complete conversion reaction between S_8 and Li_2S is generally restricted because LiPSs, the electrolyte-soluble polysulfide intermediates, diffuse from the cathode to the anode. This active loss in the cathode results in a drastic decrease in the reversible capacity. Moreover, LiPSs diffused to the anode react with the highly reactive Li metal, leading to the formation of Li_2S_2 and Li_2S solid products on the surface of the Li metal anode (Fig. 2(c)) [32]. Owing to the insulating properties of these lithium sulfides, their accumulation on the Li metal surface hampers the transport of Li^+ ions. The continuous dissolution of LiPSs into the electrolyte also increases the concentration and viscosity of the electrolyte, thereby increasing the mass transfer overpotential. It should be noted that these issues in Li-S batteries derived from the crossover of soluble LiPSs are exacerbated in practical cell operating conditions and are essential for realizing practical Li-S batteries, including high areal sulfur loading (>5 mg cm^{-2}), low electrolyte-to-sulfur (E/S) ratio (<2 μL mg^{-1}), and low negative-to-positive (N/P) ratio (<2) [33].

As a result, despite numerous studies, the cycling stability and gravimetric energy density of Li-S batteries remain insufficiently competitive for commercialization. Thus, it is of great significance to comprehensively understand the multi-effects of functional separators on Li-S electrochemistry and to develop effective functional separators that can mitigate LiPS crossover issues for the realization of advanced Li-S batteries.

MULTI-EFFECTS OF THE FUNCTIONAL SEPARATORS

The introduction of functional separators into Li-S batteries has shown a variety of desirable effects on enhancing cell performance. In particular, the functional coating layers between the separator and cathode affect the LiPS dissolution behavior and the sulfur conversion reaction at the cathode. Thus, precise control of the physical and chemical properties of functional materials coated on the separator surface enables the multi-effects of high-performance Li-S batteries to be demonstrated. In this section, the effects of the functional separators are categorized into three parts: adsorption, segregation, and electrocatalysis.

1. Adsorption Effect

The physical and chemical adsorption of electrolyte-soluble LiPSs on functional separators can enhance the Li-S cell performance. This is because the capture of LiPSs within the coating layers of functional separators inhibits the LiPS crossover from the cathode to the anode, leading to a decrease in the formation of insulating Li_2S_2 and Li_2S products on the surface of the Li metal anode. In general, there are two different adsorption mechanisms: i) physical adsorption, usually derived from van der Waals interactions; and ii) chemical adsorption induced by the formation of covalent and ionic bonds with LiPSs [34,35]. The different adsorption behaviors of LiPSs are highly dependent on the properties of functional materials. Therefore, carefully considering the functional materials is required to fabricate optimized functional separators.

1-1. Physical Adsorption

The van der Waals interaction is the most representative physical adsorption mechanism in Li-S batteries. In particular, the physical adsorption behavior of LiPSs is commonly observed in carbon-based materials, because the chemical interaction of polar LiPSs with carbon materials, whose surface properties are nonpolar, is limited.

For example, Manthiram et al. reported the fabrication of functional separators by coating conventional separators with carbon nanoparticles on conventional separators [36]. The electrolyte-soluble LiPSs was physically adsorbed on the surface of the carbon nanoparticles, suppressing the diffusion of LiPSs from the cathode to the anode (Fig. 3(a)). Moreover, the high electrical conductivity of carbon nanoparticles can act as an upper current collector of the cathode, implying that LiPSs adsorbed on the carbon nanoparticles further participate in the redox reaction to reversibly exhibit capacity (*i.e.*, reactivation reaction). As a result, a high initial discharge capacity of 1,389 mA h g^{-1} was achieved at 0.2 C rate with a carbon-nanoparticle-coated functional separator, showing outstanding cycling stability (*i.e.*, a discharge capacity of 828 mA h g^{-1} after 200 cycles).

However, despite the advantages of using carbon materials to

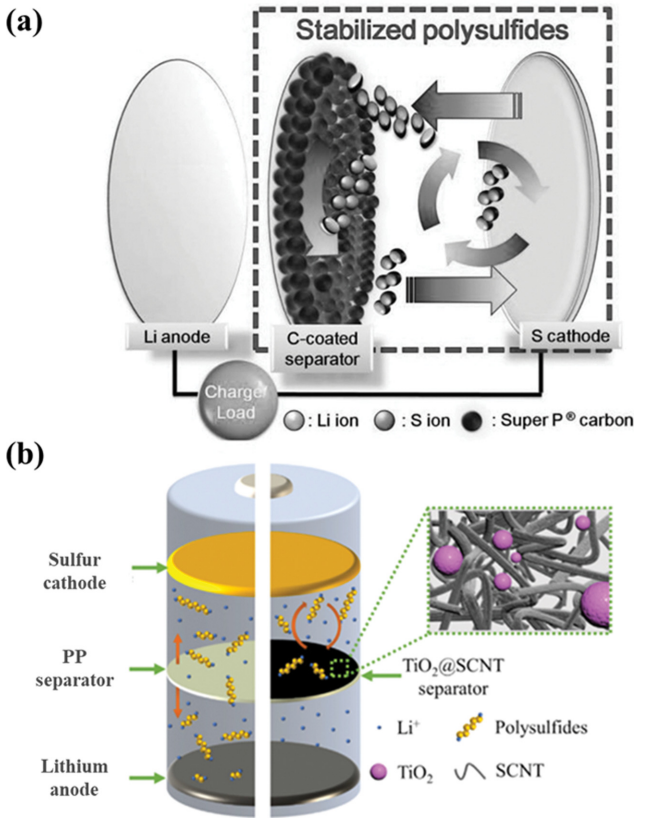

Fig. 3. (a) Graphical depiction of configuration of Li-S battery with C-coated separator (reproduced with permission from Ref. [36]). (b) Schematic illustration of beneficial effect of TiO_2@SCNT functional separator compared with PP separator (reproduced with permission from Ref. [42]).

fabricate functional separators, the physical adsorption strength between carbon and LiPSs is too weak to effectively capture large amounts of LiPSs. Considering high sulfur areal loading and long-term cycling is essential for the realization of practical Li-S batteries; the adsorption of large amounts of LiPSs by functional separators is required. In this regard, porous carbon with a high surface area is considered a promising functional material for maximizing physical adsorption.

For example, Balach et al. coated mesoporous carbon with a high surface area (843 $m^2 g^{-1}$) on the surface of a separator [37]. The number of LiPS adsorption sites significantly increased owing to the porous structures of the carbon coating materials, allowing a large amount of LiPSs to be physically captured. Moreover, it is noteworthy that porous architectures of carbon materials on separators can mitigate the volume expansion problems during the reactivation reaction of LiPSs. Consequently, mesoporous carbon-coated functional separators exhibited a high initial discharge capacity of 1,378 mA h g^{-1} at 0.2 C rate and an extremely low capacity decay per cycle of only 0.081% over 500 cycles at 0.5 C rate. Various porous carbon materials with different porous structures (*e.g.*, microporous carbon [38], hierarchically porous carbon [39], and hollow carbon [40]) have been extensively studied to fabricate functional separators for high-performance Li-S batteries. Meanwhile, the trade-off between the surface area of the separator coating layer and the E/S ratio should be carefully considered. In general, carbon materials with nonpolar surface properties are unfavorable for complete electrolyte wetting. The increase in the surface area of carbon materials deteriorates the electrolyte wetting properties of functional separators, requiring a large amount of electrolyte within the cell (*i.e.*, a high E/S ratio). Thus, the porous architecture of carbon materials and the total porosity of carbon coating layers should be precisely optimized to efficiently develop porous carbon-coated functional separators for high-performance Li-S batteries.

1-2. Chemical Adsorption

Chemical adsorption has recently been regarded as a more effective mechanism than physical adsorption to suppress the LiPS crossover through separators. This is because it exhibits a much stronger binding strength of LiPSs than physical adsorption. To build chemical bonding with LiPSs, a variety of transition metal compound materials (M_aX_b, M: metal, and X: anion), including metal oxides and sulfides, have been investigated as coating materials for separators owing to their polar surface properties which are desirable for strong chemical interactions with polar LiPSs and facile wetting of the electrolyte.

For instance, Shi et al. developed functional separators by introducing a zinc oxide (ZnO) coating layer on the surface of separators [41]. The abundant unsaturated oxygen anions (O^{2-}) and partially electron-deficient Zn metal sites in ZnO particles lead to a surface property of high polarity. Hence, the S anions and Li cations of LiPSs chemically interact with the Zn metal and O anions of ZnO, respectively. This chemical adsorption effect of the ZnO coating layer effectively suppresses the diffusion of LiPSs from the cathode to the anode during cell operation, improving the cycling stability of Li-S batteries. Furthermore, this study revealed the importance of controlling the particle dimensions of the coating materials. Among the various dimensions (from 0 to 3D) of the ZnO particles, the 1D ZnO nanotubes exhibited the most outstanding cell performance. This is attributed to the nanotube morphology offering orientational paths for facile Li^+ ion transfer and inhibiting the overgrowth of insulating Li_2S on the separator. As a result, the functional separator with ZnO nanotubes showed 927 mA h g^{-1} at 1.0 C rate even after 200 cycles. Likewise, the use of metal oxide as the coating material is a powerful strategy for fabricating advanced functional separators, but the low electrical conductivity of these metal oxide-contained materials restricts the reactivation reaction of LiPSs on the separator because of the high charge transfer resistance. In this regard, composite coating materials of metal oxides and conductive carbon materials have been considered promising for simultaneously achieving a strong chemical adsorption effect and facile reactivation of LiPSs.

Gao et al. prepared a functional separator using composite materials of titanium dioxide (TiO_2) particles and porous carbon nanotubes (SCNT) with high surface areas (Fig. 3(b)) [42]. TiO_2 is one of the most intensively studied coating materials for fabricating functional separators for high-performance Li-S batteries owing to its advantages, including facile production, low price, and eco-friendliness [43]. Furthermore, LiPSs can be strongly adsorbed on the surface of TiO_2 by the Ti-S bond. On the other hand, SCNT facilitates electron transfer throughout this composite coating layer. Therefore, LiPSs chemically adsorbed on TiO_2 can further participate in the conversion reaction, enhancing the reversible capacity. Consequently, the Li-S cell with the polypropylene (PP) separator coated by the composite of TiO_2 and SCNT (TiO_2@SCNT/PP) exhibits a high initial discharge capacity of 1,103.9 mA h g^{-1} and remarkable capacity decay per cycle of only 0.066% over 900 cycles.

Metal sulfides with layered structures (*e.g.*, MoS_2, WS_2, and SnS_2) have also been extensively investigated as coating materials for functional separators [44-47]. This is because the S^{2-} anions of metal sulfides are powerful adsorption sites for soluble LiPSs, similar to the O^{2-} anions of metal oxides. Moreover, the unsaturated metal and S atoms at the edge sites of layered structured metal sulfides exhibit unique LiPS adsorption behavior.

For instance, Manthiram's group reported molybdenum disulfide nanoparticle (MoS_2-NPs) coated separator (Fig. 4(a) and (b)) [44]. Compared to the commercial bulk MoS_2 particles, the synthesized MoS_2-NPs showed a low interlayer spacing (0.55 nm) and thickness, as demonstrated by the crystalline peak shift of the X-ray diffraction (XRD) patterns and the red-shift of the $^1E_{2g}$ and A_{1g} peaks of Raman spectroscopy, respectively (Fig. 4(c) and (d)). Cyclic voltammetry (CV) of functional separators of MoS_2-NPs exhibited a higher current density and lower overpotential than those of functional separators of commercial MoS_2 (Fig. 4(e) and (f)). Furthermore, during the ten cycles, MoS_2-NPs did not show an obvious decrease in the current densities of the cathodic and anodic peaks, whereas commercial MoS_2 showed a drastic decrease, indicating that MoS_2-NPs are desirable coating materials for enhancing the redox kinetics and reversibility of the LiPS conversion reaction throughout the separator coating layers. This is because the number of exposed edge sites of MoS_2-NPs is much higher than that of commercial bulk MoS_2. Therefore, precise control of particle size is important for developing effective layered-metal-sulfide-based coating materials for functional separators.

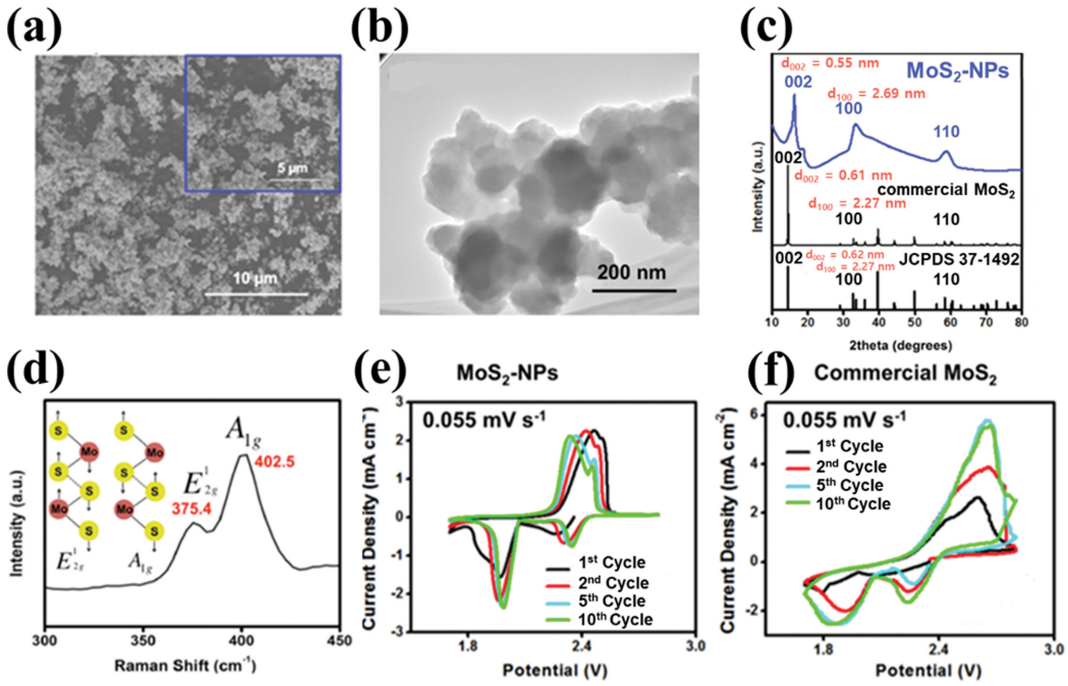

Fig. 4. (a) Microstructure of MoS_2-NPs *via* SEM analysis. (b) Transmission electron microscopy (TEM) analysis result of MoS_2-NP. (c) Comparison between MoS_2-NP and commercial MoS_2 powder *via* XRD analysis. (d) Micro-Raman analysis of MoS_2-NP loose powder with the value of A_{1g} and E_{2g} from Raman-active mode. CV test of Li-S cell at scan rate of 0.055 mV s^{-1} with (e) MoS_2-NP modified separator and (f) commercial MoS_2 modified separator (Reprinted with permission from Ref. [44]. Copyright {2018} American Chemical Society).

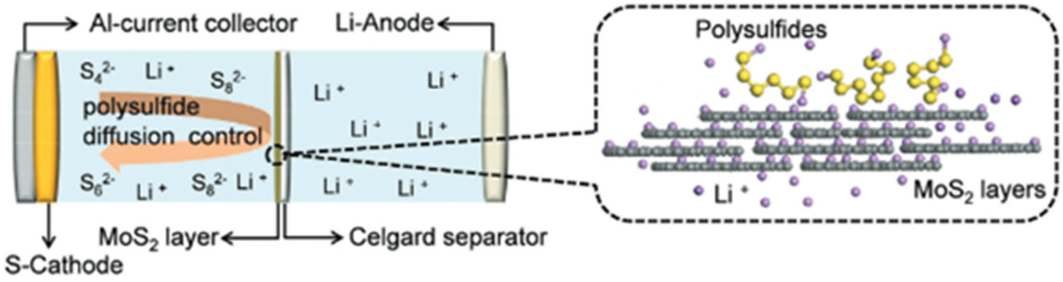

Fig. 5. Schematic diagram of Li-S battery with MoS_2/Celgard separator, which is a physical barrier of polysulfides (reproduced with permission from Ref. [55]).

2. Segregation Effect

The segregation effect is another strategy to prevent LiPSs from passing through the separators during cell operation. In contrast to the adsorption effects that inhibit LiPS crossover by physically and chemically capturing the soluble LiPSs, segregation effects block LiPS crossover by physical confinement and electrostatic repulsion.

2-1. Physical Confinement

Owing to the size difference between Li^+ ions and soluble LiPSs, careful control of the pore size of the coating materials on the surface of the separators enables the selective transport of Li^+ ions through the separators [48-50].

In this regard, metal-organic framework (MOF)-based materials have been widely used as molecular sieves owing to their well-developed ordered micropores and facile tunability of pore size [51,52]. Zhou et al. developed a functional separator using an MOF with a micropore of 0.9 nm, which is much smaller than the soluble LiPSs [1,53,54]. This unique porous structure of the MOF blocks the diffusion of LiPSs. Therefore, LiPSs are physically confined to the cathode, whereas Li^+ ions are selectively transported throughout the MOF particles. Furthermore, the additional use of graphene oxide (GO) with the MOF increased the mechanical properties of the MOF-based coating layer, which is desirable for fabricating defect-free functional separators. The physical confinement effect of LiPSs by microporous MOF coating materials, the high initial discharge capacity of 1,207 mA h g^{-1}, and the outstanding cycling stability (discharge capacity of 855 mA h g^{-1} after 1500 cycles) were achieved.

In addition to controlling the porous structure of the coating materials, thin 2D nanosheet particles can also realize the physical confinement effect of LiPSs for high-performance Li-S batteries.

For instance, 2D MoS_2 with a thickness of 350 nm was coated on the surface of a separator, as reported by Tang's group (Fig. 5) [55]. The dense coating layer induced by the stacking of 2D MoS_2 physically blocks the transport of soluble LiPSs, whereas introduces high Li^+ ion conductivity and transference number on the surface of MoS_2 to facilitate Li^+ ion diffusion. Consequently, an open circuit voltage (OCV) of 2.38 V was well maintained in the case of the Li-S cell with MoS_2 coated functional separator, implying a suppressed self-discharge phenomenon owing to the physical confinement effect of the dense MoS_2 coating layers. In addition, the Li-S cell with the as-fabricated MoS_2 coated separators exhibited a high discharge capacity of 808 mA h g^{-1} in the first cycle at 0.5 C rate. During long-term cell operation over 600 cycles, the capacity decay per cycle was only 0.083%.

2-2. Electrostatic Repulsion

In general, soluble LiPSs exhibit a negative charge because the number of S^- anions is higher than that of Li^+ cations in their molecules. Therefore, developing functional separator coated materials with negatively charged functional groups (*e.g.*, SO_3^- and COO^-) is one of the most studied strategies to inhibit the LiPS crossover. This is because the electrostatic repulsion force between negatively charged LiPSs and coating materials allows soluble LiPSs to be confined to the cathode part without severe crossover throughout the separator [56]. Furthermore, negatively charged coating materials on the separator also improve the transfer behavior of positively charged Li^+ ions, thereby decreasing the mass transfer resistance within the cell.

For example, Wei et al. introduced a negatively charged sulfonate functional group (SO_3^-) on the separator surface by coating it with a Nafion solution [57]. Based on the rate performance and CV data, it was found that the Nafion-coated separators exhibit highly stable characteristics. The capacity retention was enhanced by 90% when the current density was increased to a 5.0 C rate and then set back to a 0.2 C rate, and the cathodic peaks were highly overlapped. The cell with Nafion-coated separators of 1 μm thickness delivered a highly enhanced cycling stability with a capacity decay rate of only 0.08% per cycle over 500 cycles at 1.0 C rate.

Yim et al. proposed a dipole-aligned functional separator with ferroelectric barium titanium oxide ($BaTiO_3$, BTO) using a simple dip-coating method [58]. Under an electric field, a permanent dipole was generated inside the BTO particles aligned in the direction of the electric field, and the dipole remained even in the absence of an external electric field. The BTO-coated separator could restrict the diffusion of polysulfides across the separator through electrostatic repulsive force and suppress thermal shrinkage, which is an issue with the routine polyethylene (PE) separator in Li-S batteries (Fig. 6(a)). Overcharging was alleviated in the case of the BTO-coated separator with an enhanced initial CE of 42.3% compared to that of the pristine PE separator (26.3%) in the absence of the $LiNO_3$ additive. Scanning electron microscopy (SEM) analysis (Fig. 6(b)) revealed that the pores in the pristine PE separator clogged after 50 cycles, exacerbating the Li^+ ion conductivity of 0.035 mS cm^{-1} (90.9% before cycling) and Gurley number of 1,062.5 s 100 cc^{-1} (466.7% before cycling), which expresses the degree of air permeability of the separators. On the other hand, the PE-poled BTO separator, which prevents the diffusion of polysulfides, showed a

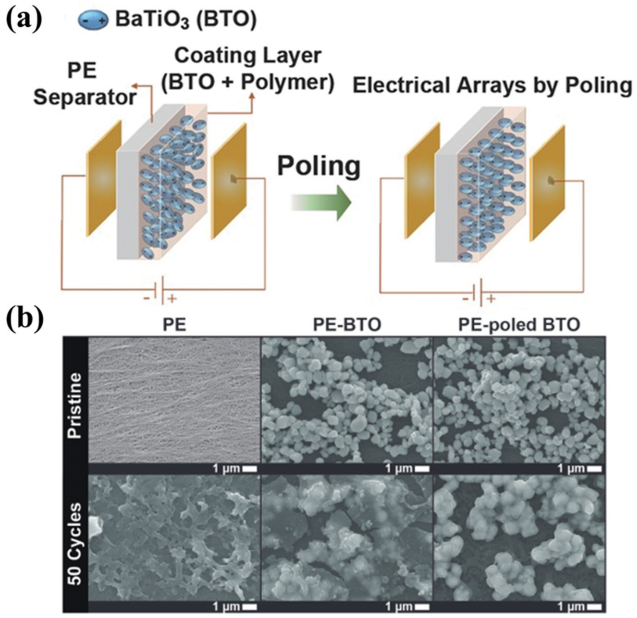

Fig. 6. (a) Schematic diagram of poling of $BaTiO_3$ (BTO) on PE separator. (b) Surface morphology comparison between PE, PE-BTO, and PE-poled BTO from SEM analysis before and after 50 cycles (reproduced with permission from Ref. [58]).

higher ionic conductivity of 0.141 mS cm^{-1} and a smaller Gurley number of 784.1 s 100 cc^{-1} than the bare PE separator. The cell with dipole aligned PE-poled BTO coated separator delivered a high discharge capacity of 1,122.1 mA h g^{-1} and 929.5 mA h g^{-1} after 50 cycles at 0.1 C rate.

3. Electrocatalysis Effect

Introducing an electrocatalyst into the separator improves the kinetics of the LiPS conversion [59]. Promoting the sluggish conversion from soluble LiPSs to Li_2S by adsorbing LiPSs on the surface of the electrocatalyst is desirable for improving the overall cell performance of Li-S batteries. As long as the sluggish conversion of LiPS is not addressed, the adsorbed LiPSs eventually cover the entire surface of the coating material. As a result of the saturation of the surface by LiPSs, the additional adsorption of LiPSs is limited. However, the accelerated conversion of LiPSs by electrocatalysts enhances the reactivation of LiPSs, resulting in the continuous formation of unsaturated adsorption sites. Furthermore, electrocatalysis decreases the opportunity for LiPSs to dissolve in the electrolyte, so the shuttle phenomenon can also be suppressed.

Before investigating which strategies have been adopted and which catalyst materials have been used to fabricate advanced functional separators for Li-S batteries, it is important to understand the mechanisms of electrocatalysis. The mechanisms are divided into three parts: i) the adsorption of LiPSs on the surface of electrocatalyst materials, ii) the surface diffusion of LiPSs on the surface of electrocatalysts, and iii) the redox reaction of LiPSs [60]. The adsorption of LiPSs is a prerequisite for the occurrence of electrocatalysis. Although LiPSs can be physically adsorbed by nonpolar carbon materials *via* van der Waals forces, adsorptive interactions between the adsorbent and LiPSs are relatively weak. Therefore, heteroatom doping on carbon materials [61] or different types of

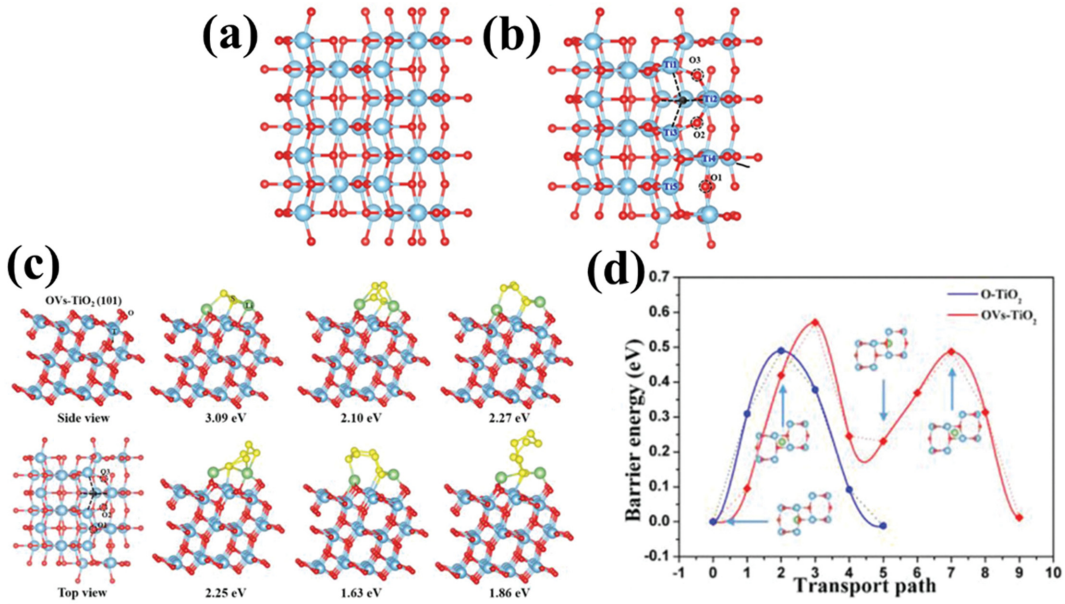

Fig. 7. Schematic illustration of structure of (a) original TiO_2 (O-TiO_2) and (b) TiO_2 with oxygen vacancies (OVs-TiO_2). (c) Calculated binding energy of OVs-TiO_2 towards polysulfides (Li_2Sx, x=3-8). (d) Calculated barrier energy of Li^+ ion migration along the Li^+ ion transport pathway (reproduced with permission from Ref. [67]).

polar transition metal compound-based electrocatalyst materials, including metal oxides [62], sulfides [63], carbides [64], and nitrides [65], have been proposed to strengthen the adsorption energy of LiPSs.

3-1. Metal Oxide

Transition metal oxides have been widely used as catalytic materials because of their chemical adsorption capability of LiPSs related to their high polarity.

Manganese dioxide (MnO_2), a transition-metal oxide, was introduced by Nazar et al. [66]. The thiosulfate functional groups formed after the first oxidation of LiPSs, accompanied by the reduction of Mn^{4+} to Mn^{2+}, can trap high-order polysulfides and facilitate the precipitation of Li_2S by disproportionation as a redox mediator. Nazar et al. suggested that the polythionate complex was created *via* the catenation of polysulfides to thiosulfate, which could trigger a conversion reaction to Li_2S. Thus, the long chain polysulfides were converted to lower polysulfides while the shuttle phenomenon was alleviated owing to the poor solubility of the polythionate complex in the electrolyte. The cell with the S/MnO_2 nanosheet composite cathode showed a highly reversible initial discharge capacity of 1,300 mA h g^{-1} at 0.2 C rate and a low capacity decay rate of only 0.036% per cycle over 2000 cycles at 2.0 C rate.

The Mai group showed that the catalytic activity and the polysulfide blocking capability could be improved by engineering oxygen vacancies, leading to excellent performance under very harsh conditions (at 2.0 C rate with a sulfur loading of 7.1 mg cm^{-2}) through a thin (500 nm) and light (0.12 mg cm^{-2}) TiO_2 nanosheet-coated functional separator with oxygen vacancy (OVs-TiO_2@PP) [67]. The structure of TiO_2 with an oxygen vacancy (OVs-TiO_2) was distinct from that of the original TiO_2 (O-TiO_2), which caused the movement of oxygen and titanium atoms around the oxygen vacancy to maintain the equilibrium of uneven electron cloud density. As a result, the polarity of OVs-TiO_2 was increased owing to the oxygen vacancy, and the binding energies of OVs-TiO_2 toward polysulfides were higher than those of O-TiO_2 (Fig. 7(a)-(c)). Although the OVs-TiO_2 coating layer was additionally introduced on the separator, facile Li^+ ion migration was verified by the low Li^+ ion migration barrier from the clamping-image-nudged elastic band (CINEB) method. The catalytic ability of the OVs-TiO_2 was enabled by the increased electrical conductivity and the binding force from the movement of the conduction band toward the Fermi level through compensation of oxygen atoms near the oxygen vacancy, in addition to the smooth Li^+ ion migration (Fig. 7(d)). The cell with the OVs-TiO_2@PP functional separator delivered an initial capacity of 802 mA h g^{-1} and retained a capacity of 631 mA h g^{-1} after 500 cycles at 2.0 C rate, while exhibiting a reversible capacity of 821 mA h g^{-1} after 100 cycles at 0.2 C rate with a sulfur loading of 7.1 mg cm^{-2}.

However, most metal oxides have been restricted by low conductivity. Therefore, the generation of oxygen deficiency and the composition with conductive carbon materials were treated as potential methods to catalyze the conversion reactions.

3-2. Metal Sulfide

Metal sulfides are widely known for their excellent performance in promoting the sluggish conversion reaction of polysulfides [68,69].

Lin et al. prepared a catalytic interlayer consisting of a metallic core and a sulfur-deficient shell with CNT(Co_9S_{8-x}/CNT) in Li-S batteries [70]. Blocking polysulfides and catalyzing the conversion reaction of polysulfides by metallic sulfur-deficient Co_9S_{8-x} with CNT was while reactivating polysulfides on the cathode side. The cell with the Co_9S_{8-x}/CNT interlayer showed better kinetics than Co_9S_8/CNT and CNT based on CV, anodic and cathodic branches of the Tafel plot in the configuration of the symmetric cell and Li-S full cell. Owing to the increased contact between the catalyst and

polysulfides with the high activity of the sulfur-deficient Co_9S_{8-x}/CNT core-shell structured catalytic interlayer, the cell delivered a low capacity decay of only 0.049% per cycle over 1000 cycles at 0.3 C rate by blocking polysulfides within the cathode side and catalyzing the conversion of polysulfides [71,72].

Xia et al. introduced zinc sulfide (ZnS) nanoparticles embedded in a 3D N-doped carbon nanosheet skeleton (NCNS) as a dual-functional separator that can alleviate the shuttle phenomenon and stabilize the Li metal anode [73]. Polysulfides and ZnS with unsaturated Zn centers and sulfur vacancies generated after carbonization of the carbon material at 750 °C formed Lewis acid-base coordination (Zn-S), leading to the chemical adsorption of polysulfides for inhibiting polysulfides. The cell with ZnS embedded in the NCNS-modified dual-functional separator showed low self-discharge behavior with a 4.1% capacity decay rate after resting for four days, and retained a discharge capacity of 922.5 mA h g^{-1} after 200 cycles.

Despite the high sulfiphilic strength of metal sulfides for capturing polysulfides, it is difficult to use metal sulfides alone owing to their limited electrical conductivity. Therefore, metal sulfides are typically combined with carbon compounds to induce rapid conversion kinetics by enhancing the electrical conductivity.

3-3. Metal Carbide

Metal carbides have been widely studied as catalysts in Li-S batteries owing to their high electrical conductivity. Unlike metal oxides and sulfides, metal carbides have been studied as catalytic materials in Li-S batteries because of their high electrical conductivity.

Peng et al. proposed a host material for conductive polar titanium carbides grown in a porous graphene framework (TiC@G). Polysulfides can be chemically adsorbed by utilizing polar materials to increase the redox kinetics of Li-S batteries. However, the role of electrical conductivity in the gradual redox kinetics of Li-S batteries remains unclear. Appropriate binding with polysulfides and facile charge transfer is enabled using polar and electrically conductive materials, leading to interfacial electrochemical kinetics [74]. In the case of nonpolar carbon as a host, the binding force toward polysulfides is insufficient, leading to limited coverage of polysulfides. Polysulfides can be easily bound to the surface of polar insulators and semiconductors; however, direct conversion to polar host materials is challenging owing to the poor electrical conductivity of polysulfides (Fig. 8(a)-(c)). The cell with polar conductive TiC@G as the host material delivered improved electrochemical performance compared to the semiconducting TiO_2@G, which requires an extra surface diffusion step.

Sun et al. prepared a molybdenum carbide (Mo_2C)-modified separator *via* simple carburization for high chemical adsorption of polysulfides and rapid redox kinetics of LiPSs [75]. The activation overpotential during precipitation to Li_2S decreased, and the reduc-

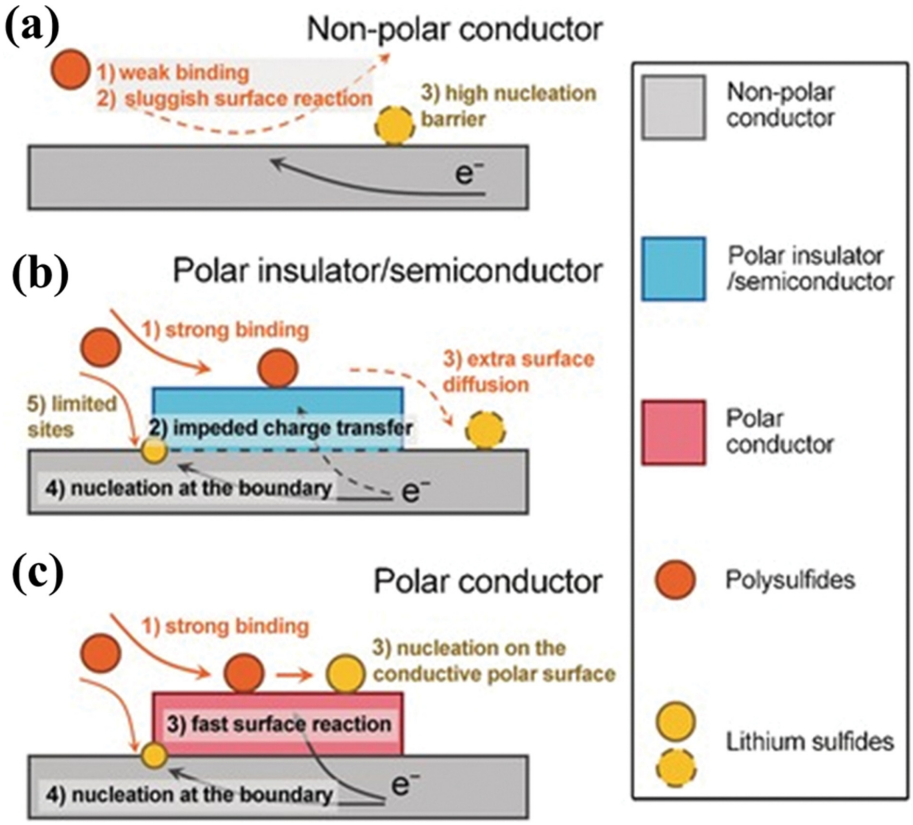

Fig. 8. Schematic diagram of electrochemical reaction kinetics depending on polarity and electrical conductivity of materials in Li-S batteries. (a) Weak binding strength with polysulfides on non-polar conductor. (b) Sufficient binding strength with polysulfides and insufficient surface diffusion on polar insulator/semiconductor. (c) Facile electrochemical kinetics of polysulfides on polar conductor (reproduced with permission from Ref. [74]).

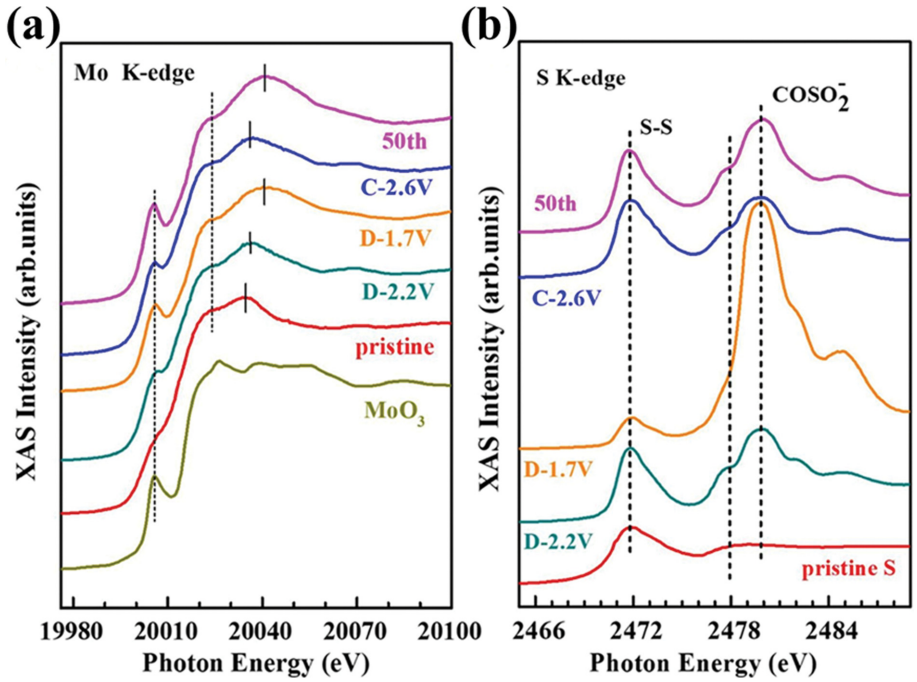

Fig. 9. Ex-situ XANES analysis data of (a) Mo K-edge, and (b) S K-edge for exploring the mechanism of polysulfide conversion reaction on KB/MoS_2 coated separator during 1st discharge/charge cycle and after 50 cycles (reproduced with permission from Ref. [75]).

tion of polysulfides was facilitated by catalytic Ketjen Black/molybdenum carbide (KB/Mo_2C). X-ray absorption near edge structure (XANES) analysis was conducted to investigate the reaction mechanism of Mo_2C and LiPSs during charging and discharging. It was found that a stable C-Mo-S bond was formed *via* the strong interaction between Mo_2C and LiPSs from the shifted peaks of the Mo K-edge and S K-edge during charging and discharging (Fig. 9(a) and (b)) [76,77]. The cell with KB/Mo_2C modified separator retained a high areal capacity of 5.2 mA h cm^{-2} after 60 cycles, corresponding to 87% of the initial reversible discharge capacity in high sulfur loading of 6.5 mg cm^{-2} at 0.1 C rate.

However, high temperatures are required during the preparation process for metal carbides, resulting in inhomogeneous active sites for trapping polysulfides by aggregation of metal carbide particles.

3-4. Metal Nitride

Unlike metal oxides and sulfides, metal nitrides have also been studied as catalytic materials in Li-S batteries owing to their high electrical conductivity.

Zhang et al. introduced an indium nitride (InN) nanowire-modified separator [78]. Because InN has a narrow band gap, it shows metallic properties and can strongly adsorb polysulfides, promoting slow polysulfide conversion reactions to restrict the shuttle phenomenon. The chemical adsorptive ability of polysulfides was verified in XPS, showing the downshifted peaks ($3d_{3/2}$ and $3d_{5/2}$) of the In element and upshifted N1s peak through the interaction between In-S and N-Li, respectively. The catalytic behavior of the InN-modified separator was confirmed with higher current intensity from CV curves and low charge transfer resistance from electrochemical impedance spectroscopy (EIS) plots. The Li-S batteries with this polar bifunctional InN-modified separator exhibited a high reversible discharge capacity of 1,430.3 mA h g^{-1} and superior cycling stability with a low capacity decay ratio of only 0.015% per cycle over 1000 cycles.

Qi et al. introduced a separator modified with mesoporous titanium nitride (MTN) microspheres [79]. TiN has been reported to exhibit reversible utilization of sulfur and superior rate performance owing to its high electrical conductivity and ability to adsorb LiPSs [80,81]. The cell with the MTN-modified separator effectively alleviates the shuttle phenomenon by using the mesoporous spherical structure as an extra physical barrier for polysulfides. Moreover, a highly conductive MTN could act as an upper current collector by reactivating captured polysulfides, resulting in a high reversible capacity and excellent rate performance. A cell with a MTN-modified separator showed a high initial reversible discharge capacity of 979 mA h g^{-1} at 0.5 C rate and retained 75%. In addition, a high discharge capacity of 672 mA h g^{-1} was realized with the MTN-modified separator at 3.0 C rate.

Metal nitrides that show high electrical conductivity can chemically adsorb polysulfides, but they are difficult to use in practical applications owing to their high temperature, long processing time, and toxic nitrogen sources for preparing metal nitrides [82].

3-5. Single Atom Catalyst

Single-atom catalysts (SACs), which are composed of atomically dispersed metal atoms on proper support, have recently received much attention owing to their excellent catalytic behavior with superior atomic efficiency and high selectivity [83-85].

Cui et al. proposed a vanadium single-atom catalyst on N-doped graphene (SAV@NG), which showed the smallest Li_2S decomposition barrier of 1.10 eV and a small Li^+ diffusion barrier compared to other materials (graphene (G), N-doped graphene (NG), or single atoms Co, V, Fe, Mn, Ru, Zn) *via* DFT calculations (Fig.

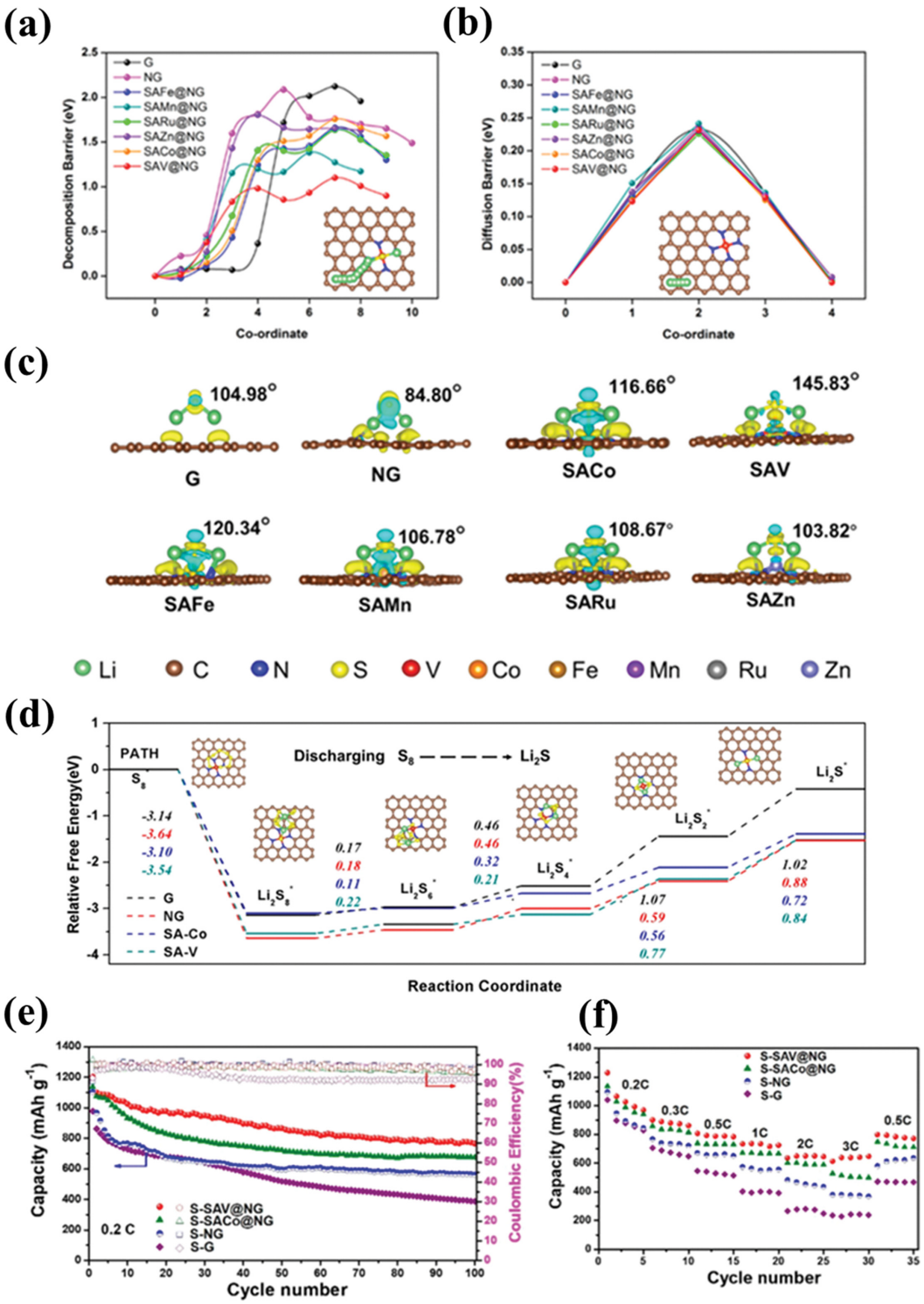

Fig. 10. (a) Decomposition barrier and (b) Li^+ ion diffusion barrier of Li_2S with various single atom catalysts on NG, and G and NG by DFT calculation. (c) Calculated result of bond length (Li-S-Li) in Li_2S and charge density when Li_2S molecule is adsorbed on the various materials from simulation. (d) Calculated energy profile of active materials (S_8 to Li_2S) during discharging process. (e) Cycling performance of the cell with various composition of cathode over 100 cycles at 0.2 C rate. (f) Rate performance of the cell with SAV@NG catalyst (Reprinted with permission from Ref. [86]. Copyright {2020} American Chemical Society).

10(a) and (b)) [86]. As the values of the Li^+ diffusion barrier were similar, it was apparent that breaking the Li-S bond in Li_2S was the dominant step in the decomposition of Li_2S during the charging process. The weak bonding strength of Li-S in the case of SAV@NG was verified by calculating the shortest bond length (Li-S) and the smallest bond angle (Li-S-Li) after adsorbing Li_2S on the substrate

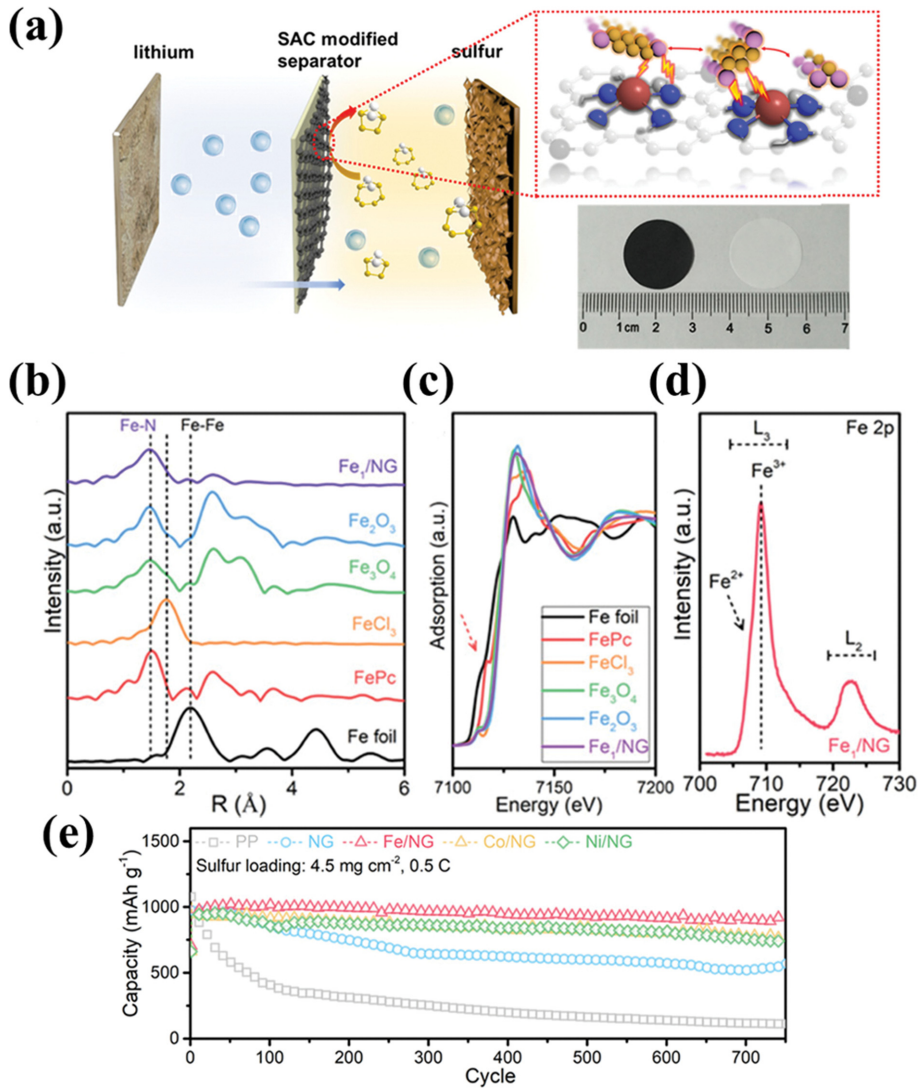

Fig. 11. (a) Schematic configuration of Li-S battery with SAC modified separator which catalyzes sluggish conversion of polysulfides. Fourier transformed data from Fe K-edge (b) EXAFS and (c) XANES of Fe-NG functional separator. (d) Analysis data of Fe-NG functional separator from Fe L-edge XAS spectrum. (e) Long term cycling performance of the cell with Fe-NG modified separator compared with other single atom modified separator over 750 cycles at 0.5 C rate (reproduced with permission from Ref. [87]).

(Fig. 10(c)). In addition, the Gibbs energy barrier of the rate-determining step from Li_2S_2 to Li_2S was sufficiently low to promote the reduction reaction based on the energy profile of the active material on the substrate during the discharge process (Fig. 10(d)). Owing to the smooth formation and decomposition of Li_2S by SAC@NG, the amount of dead Li_2S could be decreased by the enhanced utilization of active materials, resulting in improved electrochemical performance. Li-S batteries with S-SAC@NG as the cathode showed excellent coulombic efficiency of nearly 100%, a high reversible discharge capacity of 1,143 mA h g^{-1} at 0.2 C rate, and excellent rate performance even at 3.0 C rate (Fig. 10(e) and (f)).

Xie et al. prepared Fe single-atom catalysts on N-doped graphene (Fe/NG)-modified separator (Fig. 11(a)) [87]. Immobilization of polysulfides on the cathode side and rapid redox kinetics of the active material were enabled by even a small metal loading of ~2 μg in the entire cell. Extended X-ray absorption fine structure (EXAFS) analysis showed the atomic dispersion of Fe from the lack of an Fe-Fe coordination peak from the metallic Fe cluster. XANES analysis verified the highly oxidized state of Fe (Fe^{3+}) in Fe/NG, implying strong coordination of Fe with nearby nitrogen atoms (Fig. 11(b)-(d)). The adsorptive ability of the Fe/NG-modified separator toward polysulfides was validated by the high adsorption energy and decreased distance between Fe and S and N-Li *via* DFT calculations. Effective Fe single-atom catalysts, which adsorb polysulfides and promote the conversion reaction, contribute to the excellent electrochemical performance of 83.7% capacity retention after 750 cycles at 0.5 C rate even in the case of a high sulfur loading of 4.5 mg cm^{-2} (Fig. 11(e)).

3-6. Summary of the Electrocatalysis Effect

The shuttle phenomenon of soluble LiPSs caused by sluggish kinetics could be efficiently avoided by adopting an efficient electrocatalyst to a separator. The electrocatalytic behavior of Li-S bat-

teries consists of three steps: i) LiPSs should be effectively adsorbed on the surface of the electrocatalytic material, ii) LiPSs should be successfully diffused on the electrocatalyst surface, and iii) LiPSs should undergo an electrochemical reaction.

As mentioned, studies using various transition metal compound-based electrocatalysts such as metal oxides, sulfides, carbides, and nitrides which can adsorb LiPSs *via* chemical adsorption have been widely reported. Each material has its advantages and disadvantages. Metal oxides and sulfides can strongly adsorb LiPSs, but they have insulating properties. Metal nitrides and carbides have electrically conductive properties and the ability to chemically bond with LiPSs; however, there are practical problems regarding their toxic nitrogen sources and inhomogeneous active sites at high temperatures during the preparation process, respectively. The active sites of single-atom catalysts are entirely exposed, enabling maximum utilization and the promotion of electrochemical reactions even with relatively small amount of electrocatalysts; however, carrying out a rigorous preparation and characterization is challenging.

Therefore, it is necessary to screen various materials that simultaneously demonstrate proper adsorption with LiPSs and excellent electrical conductivity, and to design a process to prepare catalytic materials in a straightforward and mass-produced manner; this would help in the development of a functional separator with an efficient catalytic material to enhance the electrochemical reaction.

Lastly, to maximize the energy density of Li-S batteries, it is necessary to reduce the amount of electrolyte. Here, the mobility of LiPSs is degraded owing to the increased viscosity of the electrolyte by soluble LiPSs, resulting in limited catalytic activity induced by the poor accessibility of LiPSs to the triple-phase boundary.

However, most previous studies on improving the performance by introducing electrocatalysts in Li-S batteries were conducted under flooded electrolyte conditions (>20 μL mg^{-1}). Therefore, through in-depth research on the factors that affect catalytic activity under lean electrolyte conditions (<5 μL mg^{-1}), a basic understanding of catalytic behavior under these conditions is needed to reduce the shuttle phenomenon and improve the cyclability and energy density of Li-S batteries.

CONCLUSION AND PERSPECTIVES

Li-S batteries are difficult to commercialize owing to the shuttle phenomenon dominantly derived from the formation of soluble LiPSs during cell operation. The LiPS crossover can be affected by two key factors: i) the sulfur loading amount of the cathode and ii) the porosity of the separator.

High sulfur loading is essential for achieving a high energy density in Li-S batteries [88]. However, the utilization of a high-sulfur-loading cathode exacerbates the LiPS crossover owing to the increased amount of soluble LiPS intermediates during cell operation. The porosity of the separator also affects LiPS crossover. The LiPS crossover is degraded further due to the severe dissolution of LiPSs when using a highly porous separator. Therefore, controlling the porosity of the coating layer on the separator is crucial for realizing high-performance Li-S batteries when designing a functional separator.

In conclusion, the design of functional separators has recently been regarded as an effective strategy for achieving high-performance Li-S batteries by inhibiting LiPS crossover in electrolyte. It has been demonstrated that the precise control of the physical (*e.g.*, particle size, dimension, and porous structures) and chemical properties (*e.g.*, adsorption strength with LiPSs, Li^+ ion surface diffusivity, and electrocatalytic activity) of functional materials on separators can address the intrinsic problems of Li-S batteries, including the shuttle phenomenon and low sulfur utilization ratio. A fundamental understanding of the role of functional separators and the relationship between the properties of separators and Li-S cell performance have been systematically elucidated during the last seven years by worldwide efforts.

However, despite the significant improvement in Li-S cell performance at the coin cell level by developing functional separators, the achievement of high gravimetric energy density (>300 W h kg^{-1} at a total capacity of A h level) and long cycling stability (>100 cycles at the practical pouch cell level) have been rarely reported so far. Therefore, several issues should be carefully considered in developing advanced functional separators for high-performance Li-S pouch cells.

First, a more detailed understanding of the relationship between the total porosity of the coating layer on the separator surface and the Li-S cell performance is required. Most previous studies have focused on the porous structures of coating materials, but the porous structures derived from interparticle voids have been overlooked so far. The diffusivities of soluble LiPSs and Li^+ ions are determined by the penetration behaviors of the electrolyte into the coating layer of the separators. Therefore, the total porosity, calculated by considering the porous structures of the coating materials and interparticle porous structures, is one of the most important parameters for determining the cell performance of Li-S batteries.

Second, the tortuosity of the coating layer is also a crucial parameter that affects the diffusion behavior of soluble LiPSs from the cathode to the anode and Li^+ ion transfer behaviors. However, the tortuosity of the coating layer is commonly overlooked when fabricating functional separators for Li-S batteries. For example, the high tortuosity of the functional coating layers can effectively inhibit the shuttle phenomenon, but the mass transfer resistance can be increased because of the poor diffusion of Li^+ ions. In contrast, the low tortuosity of the functional coating layers facilitates Li^+ ion transfer, but the severe LiPS crossover can occur. Therefore, precise control of the tortuosity of the coating layers is required with careful consideration of the Li^+ ion diffusivity and LiPS adsorption strength of the coating materials.

Third, the development of simple techniques to fabricate homogeneous large-area functional separators without defects or cracked regions is required. This large-area coating strategy is necessary for manufacturing large-area pouch cells with a practical total capacity. Moreover, a large-area coating is required for efficient large-scale industrial production.

Finally, minimization of the thickness and mass of the functional coating layers is required to maximize the volumetric and gravimetric energy densities of Li-S batteries. It should be carefully considered that a decrease in the thickness and mass of the functional coating layers leads to a decrease in the number of adsorption sites for capturing the soluble LiPSs. The increase in the specific sur-

face area of coating materials can be a breakthrough to effectively prevent the LiPS crossover phenomenon with extremely low thickness and mass of functional coating layers.

In summary, strategic guidance for the future development of advanced functional separators for high-performance Li-S batteries is as follows. 1) A fundamental understanding is required to determine which properties of the functional separator mainly affect the electrochemical performance of Li-S batteries. As described above, they can be the physical properties (i.e., particle size, dimensions, and pore structure) or chemical properties (i.e., adsorption force with LiPSs, diffusion of Li^+ ions, and electrocatalytic activity). In addition, the porosity or tortuosity of the functional coating layer on the separator is directly related to the diffusion of LiPSs and Li^+ ions. 2) The effects of alleviating the problems in Li-S batteries should be fully explored. For example, to alleviate the shuttle phenomenon, which is mainly problematic in Li-S batteries, the adsorption, segregation, and electrocatalysis effects can be utilized, as covered in this review. To suppress the lithium dendrite growth problem, uniform Li^+ ion flux induced by coating lithiophilic materials on the separator [89], ordered pore sizes of the coating layer [90], reversible lithium deposition/stripping through lithium surface modification [91], and enhanced mechanical properties by rigid coating materials [92] can be utilized. 3) An in-depth investigation of various materials that can be used to solve the target problems in Li-S batteries is needed. 4) To maximize the practical use of Li-S batteries, it should be possible to manufacture functional separators with large areas using a simple fabrication process for operation in pouch cells. In addition, they should be as light and thin as possible to maximize volumetric and gravimetric energy densities. Increasing the surface area of the coating material can be an effective solution for preventing LiPS crossover. Finally, operating a pouch cell under lean electrolyte conditions is essential to maximizing the energy density of Li-S batteries. Under lean electrolyte conditions, the mobility of soluble LiPSs is limited owing to localized electrolyte consumption by side reactions, thus improving the wettability of the functional separator with the electrolyte, which can be an important factor in the performance of Li-S batteries.

Consequently, the use of functional separators in high-performance Li-S batteries is a promising strategy. Further understanding of the correlation between the overall physical and chemical properties of functional coating layers and cell performance is required to avoid trial and error in the fabrication of multifunctional separators.

ACKNOWLEDGEMENTS

This work was supported by National Research Foundation (NRF) of Korea which is funded by Ministry of Science and ICT under grant no. 2021M3H4A1A02049893 and 2021M3D1A2051605.

REFERENCES

1. S. Bai, X. Liu, K. Zhu, S. Wu and H. Zhou, *Nat. Energy*, **1**, 1 (2016).
2. X. Lv, T. Lei, B. Wang, W. Chen, Y. Jiao, Y. Hu, Y. Yan, J. Huang, J. Chu and C. Yan, *Adv. Energy Mater.*, **9**, 1901800 (2019).
3. R. Fang, S. Zhao, Z. Sun, D. W. Wang, H. M. Cheng and F. Li, *Adv. Mater.*, **29**, 1606823 (2017).
4. J. r. G. Werner, S. S. Johnson, V. Vijay and U. Wiesner, *Chem. Mater.*, **27**, 3349 (2015).
5. J.-Q. Huang, Q. Zhang and F. Wei, *Energy Storage Mater.*, **1**, 127 (2015).
6. Y. Li, Z. Li, C. Zhou, X. Liao, X. Liu, X. Hong, X. Xu, Y. Zhao and L. Mai, *Chem. Eng. J.*, **422**, 130107 (2021).
7. R. Saroha, J.-H. Ahn and J. S. Cho, *Korean J. Chem. Eng.*, **38**, 461 (2021).
8. Z. Li, H. B. Wu and X. W. D. Lou, *Energy Environ. Sci.*, **9**, 3061 (2016).
9. T. Liu, H. Hu, X. Ding, H. Yuan, C. Jin, J. Nai, Y. Liu, Y. Wang, Y. Wan and X. Tao, *Energy Storage Mater.*, **30**, 346 (2020).
10. M. Rana, B. Luo, M. R. Kaiser, I. Gentle and R. Knibbe, *J. Energy Chem.*, **42**, 195 (2020).
11. C. Zha, J. Xiang, Y. Zhao and L. Wang, *J. Mater. Chem. A*, **10**, 10326 (2022).
12. S. Kim, W.-G. Lim, A. Cho, J. Jeong, C. Jo, D. Kang, S. M. Han, J. W. Han and J. Lee, *ACS Appl. Energy Mater.*, **3**, 2643 (2020).
13. H. Chen, Z. Wu, M. Zheng, T. Liu, C. Yan, J. Lu and S. Zhang, *Mater. Today*, **52**, 364 (2021).
14. W.-G. Lim, C. Jo, J. Lee and D. S. Hwang, *Korean J. Chem. Eng.*, **35**, 579 (2018).
15. W. G. Lim, S. Kim, C. Jo and J. Lee, *Angew. Chem.*, **131**, 18920 (2019).
16. Y. Ren, A. Bhargav, W. Shin, H. Sul and A. Manthiram, *Angew. Chem.*, **134**, e202207907 (2022).
17. W. G. Lim, C. Jo, A. Cho, J. Hwang, S. Kim, J. W. Han and J. Lee, *Adv. Mater.*, **31**, 1806547 (2019).
18. J. Kim, S. J. Kim, E. Jung, D. H. Mok, V. K. Paidi, J. Lee, H. S. Lee, Y. Jeoun, W. Ko, H. Shin, B.-H. Lee, S.-Y. Kim, H. Kim, J. H. Kim, S.-P. Cho, K.-S. Lee, S. Back, S.-H. Yu, Y.-E. Sung and T. Hyeon, *Adv. Funct. Mater.*, **32**, 2110857 (2022).
19. Z. Wang, J. Shen, X. Xu, J. Yuan, S. Zuo, Z. Liu, D. Zhang and J. Liu, *Small*, **18**, 2106640 (2022).
20. H. Yuan, X. Chen, G. Zhou, W. Zhang, J. Luo, H. Huang, Y. Gan, C. Liang, Y. Xia, J. Zhang, J. Wang and X. Tao, *ACS Energy Lett.*, **2**, 1711 (2017).
21. Z. Li, J. Zhang, B. Guan, D. Wang, L.-M. Liu and X. W. D. Lou, *Nat. Commun.*, **7**, 1 (2016).
22. N. Jayaprakash, J. Shen, S. S. Moganty, A. Corona and L. A. Archer, *Angew. Chem. Int. Ed.*, **50**, 5904 (2011).
23. W.-G. Lim, Y. Mun, A. Cho, C. Jo, S. Lee, J. W. Han and J. Lee, *ACS Nano*, **12**, 6013 (2018).
24. H. Wei, J. Ma, B. Li, Y. Zuo and D. Xia, *ACS Appl. Mater. Interfaces*, **6**, 20276 (2014).
25. G. Feng, X. Liu, Z. Wu, Y. Chen, Z. Yang, C. Wu, X. Guo, B. Zhong, W. Xiang and J. Li, *J. Alloys Compd.*, **817**, 152723 (2020).
26. H. Lin, L. Yang, X. Jiang, G. Li, T. Zhang, Q. Yao, G. W. Zheng and J. Y. Lee, *Energy Environ. Sci.*, **10**, 1476 (2017).
27. D. Wang, F. Li, R. Lian, J. Xu, D. Kan, Y. Liu, G. Chen, Y. Gogotsi and Y. Wei, *ACS Nano*, **13**, 11078 (2019).
28. H. Chen, C. Wang, W. Dong, W. Lu, Z. Du and L. Chen, *Nano Lett.*, **15**, 798 (2015).

29. Q. Jin, X. Qi, F. Yang, R. Jiang, Y. Xie, L. Qie and Y. Huang, *Energy Storage Mater.*, **38**, 255 (2021).
30. C. Shen, J. Xie, M. Zhang, P. Andrei, M. Hendrickson, E. J. Plichta and J. P. Zheng, *Electrochim. Acta*, **248**, 90 (2017).
31. C. Li, Z. Xi, D. Guo, X. Chen and L. Yin, *Small*, **14**, 1701986 (2018).
32. M. R. Busche, P. Adelhelm, H. Sommer, H. Schneider, K. Leitner and J. Janek, *J. Power Sources*, **259**, 289 (2014).
33. S. Li, W. Zhang, J. Zheng, M. Lv, H. Song and L. Du, *Adv. Energy Mater.*, **11**, 2000779 (2021).
34. P. Jovanović, M. S. Mirshekarloo, M. R. Hill, A. F. Hollenkamp, M. Majumder and M. Shaibani, *Adv. Mater. Technol.*, **6**, 2001136 (2021).
35. Y. Zhu, S. Wang, Z. Miao, Y. Liu and S. L. Chou, *Small*, **14**, 1801987 (2018).
36. S. H. Chung and A. Manthiram, *Adv. Funct. Mater.*, **24**, 5299 (2014).
37. J. Balach, T. Jaumann, M. Klose, S. Oswald, J. Eckert and L. Giebeler, *Adv. Funct. Mater.*, **25**, 5285 (2015).
38. S. H. Chung and A. Manthiram, *Adv. Mater.*, **26**, 7352 (2014).
39. C. Choi and D.-W. Kim, *J. Power Sources*, **448**, 227462 (2020).
40. M. Rana, J. Kim, L. Peng, H. Qiu, R. Kaiser, L. Ran, M. S. A. Hossain, B. Luo, I. Gentle and L. Wang, *Nanoscale*, **13**, 11086 (2021).
41. N. Shi, B. Xi, Z. Feng, F. Wu, D. Wei, J. Liu and S. Xiong, *J. Mater. Chem. A*, **7**, 4009 (2019).
42. Z. Gao, Z. Xue, Y. Miao, B. Chen, J. Xu, H. Shi, T. Tang and X. Zhao, *J. Alloys Compd.*, **906**, 164249 (2022).
43. J. Safari and S. Gandomi-Ravandi, *New J. Chem.*, **38**, 3514 (2014).
44. P. Han, S.-H. Chung and A. Manthiram, *ACS Appl. Mater. Interfaces*, **10**, 23122 (2018).
45. D. Duphil, S. Bastide and C. Lévy-Clément, *J. Mater. Chem.*, **12**, 2430 (2002).
46. O. Ogoke, G. Wu, X. Wang, A. Casimir, L. Ma, T. Wu and J. Lu, *J. Mater. Chem. A*, **5**, 448 (2017).
47. R. V. Bugga, S. C. Jones, J. Pasalic, C. S. Seu, J.-P. Jones and L. Torres, *J. Electrochem. Soc.*, **164**, A265 (2016).
48. Y. Cao, H. Wu, G. Li, C. Liu, L. Cao, Y. Zhang, W. Bao, H. Wang, Y. Yao and S. Liu, *Nano Lett.*, **21**, 2997 (2021).
49. Z. Cheng, H. Pan, J. Chen, X. Meng and R. Wang, *Adv. Energy Mater.*, **9**, 1901609 (2019).
50. J. Sun, Y. Sun, M. Pasta, G. Zhou, Y. Li, W. Liu, F. Xiong and Y. Cui, *Adv. Mater.*, **28**, 9797 (2016).
51. Y. S. Li, F. Y. Liang, H. Bux, A. Feldhoff, W. S. Yang and J. Caro, *Angew. Chem.*, **122**, 558 (2010).
52. G. Liu, V. Chernikova, Y. Liu, K. Zhang, Y. Belmabkhout, O. Shekhah, C. Zhang, S. Yi, M. Eddaoudi and W. J. Koros, *Nat. Mater.*, **17**, 283 (2018).
53. M. Vijayakumar, N. Govind, E. Walter, S. D. Burton, A. Shukla, A. Devaraj, J. Xiao, J. Liu, C. Wang and A. Karim, *Phys. Chem. Chem. Phys.*, **16**, 10923 (2014).
54. M. Cuisinier, P.-E. Cabelguen, S. Evers, G. He, M. Kolbeck, A. Garsuch, T. Bolin, M. Balasubramanian and L. F. Nazar, *J. Phys. Chem. Lett.*, **4**, 3227 (2013).
55. Z. A. Ghazi, X. He, A. M. Khattak, N. A. Khan, B. Liang, A. Iqbal, J. Wang, H. Sin, L. Li and Z. Tang, *Adv. Mater.*, **29**, 1606817 (2017).
56. X. Yu, J. Joseph and A. Manthiram, *Mater. Horiz.*, **3**, 314 (2016).
57. J.-Q. Huang, Q. Zhang, H.-J. Peng, X.-Y. Liu, W.-Z. Qian and F. Wei, *Energy Environ. Sci.*, **7**, 347 (2014).
58. T. Yim, S. H. Han, N. H. Park, M. S. Park, J. H. Lee, J. Shin, J. W. Choi, Y. Jung, Y. N. Jo and J. S. Yu, *Adv. Funct. Mater.*, **26**, 7817 (2016).
59. P. Fusheng, Y. Yuan and S. Jie, *Prog. Chem.*, **33**, 442 (2021).
60. P. Wang, B. Xi, M. Huang, W. Chen, J. Feng and S. Xiong, *Adv. Energy Mater.*, **11**, 2002893 (2021).
61. H. Yuan, W. Zhang, J.-G. Wang, G. Zhou, Z. Zhuang, J. Luo, H. Huang, Y. Gan, C. Liang, Y. Xia, J. Zhang and X. Tao, *Energy Storage Mater.*, **10**, 1 (2018).
62. Z. Zhou, Y. Li, T. Fang, Y. Zhao, Q. Wang, J. Zhang and Z. Zhou, *Nanomaterials*, **9**, 1574 (2019).
63. Y. Zhang, G. Xu, Q. Kang, L. Zhan, W. Tang, Y. Yu, K. Shen, H. Wang, X. Chu and J. Wang, *J. Mater. Chem. A*, **7**, 16812 (2019).
64. Z. Zhang, J.-N. Wang, A. Shao, D.-G. Xiong, J.-W. Liu, C.-Y. Lao, K. Xi, S.-Y. Lu, Q. Jiang and J. Yu, *Sci. China Mater.*, **63**, 2443 (2020).
65. G. Chen, X. Song, S. Wang, X. Chen and H. Wang, *J. Power Sources*, **408**, 58 (2018).
66. X. Liang, C. Hart, Q. Pang, A. Garsuch, T. Weiss and L. F. Nazar, *Nat. Commun.*, **6**, 1 (2015).
67. Z. Li, C. Zhou, J. Hua, X. Hong, C. Sun, H. W. Li, X. Xu and L. Mai, *Adv. Mater.*, **32**, 1907444 (2020).
68. Z. Yuan, H.-J. Peng, T.-Z. Hou, J.-Q. Huang, C.-M. Chen, D.-W. Wang, X.-B. Cheng, F. Wei and Q. Zhang, *Nano Lett.*, **16**, 519 (2016).
69. J. Xu, W. Zhang, H. Fan, F. Cheng, D. Su and G. Wang, *Nano Energy*, **51**, 73 (2018).
70. H. Lin, S. Zhang, T. Zhang, S. Cao, H. Ye, Q. Yao, G. W. Zheng and J. Y. Lee, *ACS Nano*, **13**, 7073 (2019).
71. H. Li, C. Tsai, A. L. Koh, L. Cai, A. W. Contryman, A. H. Fragapane, J. Zhao, H. S. Han, H. C. Manoharan and F. Abild-Pedersen, *Nat. Mater.*, **15**, 48 (2016).
72. H. Wang, Q. Zhang, H. Yao, Z. Liang, H.-W. Lee, P.-C. Hsu, G. Zheng and Y. Cui, *Nano Lett.*, **14**, 7138 (2014).
73. Z. Li, F. Zhang, L. Tang, Y. Tao, H. Chen, X. Pu, Q. Xu, H. Liu, Y. Wang and Y. Xia, *Chem. Eng. J.*, **390**, 124653 (2020).
74. H. J. Peng, G. Zhang, X. Chen, Z. W. Zhang, W. T. Xu, J. Q. Huang and Q. Zhang, *Angew. Chem. Int. Ed.*, **55**, 12990 (2016).
75. M. He, X. Li, W. Li, M. Zheng, J. Wang, S. Ma, Y. Ma, G. Yin, P. Zuo and X. Sun, *Chem. Eng. J.*, **411**, 128563 (2021).
76. Y. Kim, D. H. Jackson, D. Lee, M. Choi, T. W. Kim, S. Y. Jeong, H. J. Chae, H. W. Kim, N. Park and H. Chang, *Adv. Funct. Mater.*, **27**, 1701825 (2017).
77. L. Cai, J. He, Q. Liu, T. Yao, L. Chen, W. Yan, F. Hu, Y. Jiang, Y. Zhao and T. Hu, *J. Am. Chem. Soc.*, **137**, 2622 (2015).
78. L. Zhang, X. Chen, F. Wan, Z. Niu, Y. Wang, Q. Zhang and J. Chen, *ACS Nano*, **12**, 9578 (2018).
79. B. Qi, X. Zhao, S. Wang, K. Chen, Y. Wei, G. Chen, Y. Gao, D. Zhang, Z. Sun and F. Li, *J. Mater. Chem. A*, **6**, 14359 (2018).
80. Z. Hao, L. Yuan, C. Chen, J. Xiang, Y. Li, Z. Huang, P. Hu and Y. Huang, *J. Mater. Chem. A*, **4**, 17711 (2016).
81. D.-R. Deng, J. Lei, F. Xue, C.-D. Bai, X.-D. Lin, J.-C. Ye, M.-S. Zheng and Q.-F. Dong, *J. Mater. Chem. A*, **5**, 23497 (2017).
82. Y. Zhang, B. Ouyang, J. Xu, G. Jia, S. Chen, R. S. Rawat and H. J. Fan, *Angew. Chem.*, **128**, 8812 (2016).
83. H. Xu, D. Cheng, D. Cao and X. C. Zeng, *Nat. Catal.*, **1**, 339 (2018).
84. L. Liu and A. Corma, *Chem. Rev.*, **118**, 4981 (2018).

85. Z. Pu, I. S. Amiinu, R. Cheng, P. Wang, C. Zhang, S. Mu, W. Zhao, F. Su, G. Zhang and S. Liao, *Nano-Micro Lett.*, **12**, 1 (2020).
86. G. Zhou, S. Zhao, T. Wang, S.-Z. Yang, B. Johannessen, H. Chen, C. Liu, Y. Ye, Y. Wu, Y. Peng, C. Liu, S. P. Jiang, Q. Zhang and Y. Cui, *Nano Lett.*, **20**, 1252 (2019).
87. K. Zhang, Z. Chen, R. Ning, S. Xi, W. Tang, Y. Du, C. Liu, Z. Ren, X. Chi and M. Bai, *ACS Appl. Mater. Interfaces*, **11**, 25147 (2019).
88. M. Zhao, B.-Q. Li, X.-Q. Zhang, J.-Q. Huang and Q. Zhang, *ACS Cent. Sci.*, **6**, 1095 (2020).
89. Y. Liu, S. Xiong, J. Wang, X. Jiao, S. Li, C. Zhang, Z. Song and J. Song, *Energy Storage Mater.*, **19**, 24 (2019).
90. C.-L. Song, Z.-H. Li, L.-Y. Ma, M.-Z. Li, S. Huang, X.-J. Hong, Y.-P. Cai and Y.-Q. Lan, *ACS Nano*, **15**, 13436 (2021).
91. Z. Hu, F. Liu, J. Gao, W. Zhou, H. Huo, J. Zhou and L. Li, *Adv. Funct. Mater.*, **30**, 1907020 (2020).
92. Z. Zhou, B. Chen, T. Fang, Y. Li, Z. Zhou, Q. Wang, J. Zhang and Y. Zhao, *Adv. Energy Mater.*, **10**, 1902023 (2020).

Jinwoo Lee obtained B. S., M. S., and Ph.D. from the Department of Chemical and Biological Engineering at Seoul National University. After postdoctoral work at Seoul National University (with Prof. Taeghwan Hyeon) and Cornell University (with Prof. Ulrich Wiesner), he served as a professor of Chemical Engineering at Pohang University of Science and Technology (POSTECH) (2008-2018). In 2018, he was appointed as a professor of the Department of Biomolecular and Chemical Engineering at Korea Advanced Institute of Science and Technology (KAIST). His main research concern is the synthesis and application of nano-functional materials for energy conversion and storage devices.